Magnetic flux induced spin polarization in semiconductor multichannel rings with Rashba spin-orbit coupling

G. S. Lozano[1,*] and M. J. Sánchez[2,†]
[1]*Departamento de Física, FCEyN, Universidad de Buenos Aires, 1428 Ciudad de Buenos Aires, Argentina*
[2]*Centro Atómico Bariloche, Comisión Nacional de Energía Atómica, 8400 San Carlos de Bariloche, Argentina*
(Received 20 September 2005; published 9 November 2005)

We show that a finite magnetic flux threading a multichannel semiconductor ring can induce spin polarization at the borders of the sample when the Rashba spin-orbit interaction is taken into account. The spin polarization has an opposite sign on the two borders giving rise to a spin accumulation effect in the absence of external electric fields or currents. In addition the persistent charge current (PC) is investigated. As a consequence of the multichannel nature of the ring, the signature of the spin-orbit interaction in the PC cannot be encoded in a single effective topological phase.

DOI: 10.1103/PhysRevB.72.205315 PACS number(s): 72.25.Dc, 73.23.Ra

I. INTRODUCTION

In recent years semiconductor devices in which the spin orbit (SO) interaction plays a significant role, have been proposed for applications in spin controlled transport.[1] Among them, multiple connected mesoscopic geometries are natural candidates to explore how spin dependent effects manifest in the quantum interference patterns that appear in transport measurements at low temperatures.[2–4] In the case of quasi-one-dimensional (quasi-1D) rings, the effect of the SO interaction has been addressed theoretically in a series of papers.[5–7] As a consequence of the SO, the wave function acquires a nontrivial spin dependent topological phase[8] that manifests in several remarkable quantum phenomena.

We will be considering SO coupling of the Rashba type which arises on a two-dimensional electron gas (2DEG) of a semiconductor heterostructure due to the inversion asymmetry of the confining potential.[9] When a ring is pierced by a magnetic flux, the SO modifies the magnetic flux dependence of the spectrum and therefore the conductance[10] and the persistent current (PC), in the case of an isolated ring, change as compared to the case without SO.[11] So far the theoretical analysis has been restricted to 1D geometries and quasi-1D in the two band approximation,[12] where the results are qualitatively the same as in the 1D systems. The multichannel nature of realistic rings employed in the experiments[13,14] and recent controversies around the possibility of an experimentally observed spin dependent phase in transport experiments with many propagating modes[15,16] challenges us to address exactly the 2D geometry.

In this work we show that when a multichannel ring with Rashba SO coupling is pierced by a magnetic flux a spin accumulation effect is developed on the boundaries of the sample. In addition, even for an even number of electrons, a finite spin polarization in the direction perpendicular to the plane of the ring is generated whose intensity can be controlled with the magnetic flux. These phenomena share some analogies with the intrinsic spin Hall effect (SHE) studied in bar or T-like geometries,[17–19] but in the present case the system is in equilibrium without external electric fields or voltage drops applied.[20]

II. MULTICHANNEL RING WITH RASHBA SO INTERACTION

We start by considering a 2D electron gas in the xy plane confined to a mesoscopic annular region (multichannel ring) threaded by a magnetic flux Φ. The single particle Hamiltonian describing an electron of effective mass m subject to the Rashba SO coupling reads

$$H=\frac{\mathbf{p}^2}{2m}+V+\frac{\alpha}{\hbar}(\mathbf{p}\times\hat{\sigma})\cdot\hat{z}, \tag{1}$$

where α is the strength of the Rashba spin orbit (RSO) coupling and the Pauli matrices $\hat{\sigma}$ are defined as standard. Employing polar coordinates ρ and φ, the hard wall confining potential defining the ring is

$$V(\rho)=\begin{cases}0 & \text{for } r<\rho<R\\ \infty & \text{otherwise,}\end{cases} \tag{2}$$

where r and R are the internal and external radii of the ring. The vector potential which is introduced in the Hamiltonian via the substitution, $\mathbf{p}=\hbar\mathbf{k}=-i\hbar\nabla-e/c\mathbf{A}$, is written in the axial gauge as $\mathbf{A}=(\Phi/2\pi\rho)\hat{\varphi}$. Using, $\hat{\sigma}_\rho=\cos\varphi\hat{\sigma}_x+\sin\varphi\hat{\sigma}_y$ and $\hat{\sigma}_\varphi=-\sin\varphi\hat{\sigma}_x+\cos\varphi\hat{\sigma}_y$ we can rewrite the Hamiltonian as

$$H=-\frac{\hbar^2}{2m}\left[\frac{1}{\rho}\partial_\rho(\rho\partial_\rho)-\frac{1}{\rho^2}(i\partial_\varphi+\nu)^2\right]$$
$$+i\alpha\hat{\sigma}_\varphi\partial_\rho-\frac{\alpha}{\rho}\hat{\sigma}_\rho(i\partial_\varphi+\nu), \tag{3}$$

where $\nu=\Phi/\Phi_0$ is the magnetic flux in units of the flux quantum $\Phi_0=hc/e$. As $J_z=l_z+s_z=-i\hbar\partial_\phi+\frac{1}{2}\hbar\hat{\sigma}_z$, commutes with H, the eigenfunctions can be chosen as

$$\psi_j(\rho,\varphi)=\begin{bmatrix}e^{i(l)\varphi}\tilde{f}_l(\rho)\\ e^{i(l+1)\varphi}\tilde{g}_{l+1}(\rho)\end{bmatrix}. \tag{4}$$

where $J_z\psi_j=\hbar j\psi_j$ and $j=l+\frac{1}{2}$. In what follows it will be useful to work with dimensionless variables. With that purpose we define the dimensionless coordinate $\xi=\rho/R$, the aspect ratio $\lambda=R/r$ and

$$\epsilon = \frac{2mER^2}{\hbar^2} \equiv \frac{E}{E_0}, \quad \beta = 2R\frac{\alpha m}{\hbar^2}, \quad f_l = R\tilde{f}_l, \quad g_l = R\tilde{g}_l, \tag{5}$$

with the boundary conditions

$$f_l(\lambda^{-1}) = g_{l+1}(\lambda^{-1}) = 0 = f_l(1) = g_{l+1}(1). \tag{6}$$

We can look solutions of the form $f_l(\xi) \sim Y_{l-\nu}(k\xi)$ and $g_{l+1}(\xi) \sim Y_{l+1-\nu}(k\xi)$ where $Y_l(\xi)$ are Bessel functions of the type $J_l(\xi)$ or $N_l(\xi)$. The Rashba term simply acts as rising or lowering operator on the Bessel function basis since the following standard recurrence relations hold:[21]

$$\left(\frac{d}{d\xi} + \frac{1 \pm l}{\xi}\right) Y_{l\pm1}(k\xi) = \pm k Y_l(k\xi). \tag{7}$$

This is indeed the property which allows us to obtain, as in the case of a disk geometry,[22] an exact analytical solution. Due to the RSO, the bulk spectrum has two branches

$$\epsilon = k^2 \pm \beta k. \tag{8}$$

Therefore for a given value of ϵ there are two nontrivial solutions for the momentum k that we denote k^+ and k^-, respectively. It is then possible to obtain a solution as

$$Y(\xi) = \begin{pmatrix} f_l \\ g_{l+1} \end{pmatrix} = \sum_{i=1}^{4} c_i Y_i(\xi) = \sum_{i=1}^{4} c_i \begin{pmatrix} Y_i^1 \\ Y_i^2 \end{pmatrix} \tag{9}$$

with

$$Y_1(\xi) = \begin{pmatrix} J_{l-\nu}(k^+\xi) \\ J_{l-\nu+1}(k^+\xi) \end{pmatrix}, \quad Y_2(\xi) = \begin{pmatrix} J_{l-\nu}(k^-\xi) \\ -\frac{|\epsilon|}{\epsilon} J_{l-\nu+1}(k^-\xi) \end{pmatrix}$$

and with Y_3 and Y_4 obtained from Y_1 and Y_2 by exchanging Bessel functions of type J by Bessel functions of type N.

Defining $\tilde{Y}$ as

$$\tilde{Y} = \begin{pmatrix} Y_1^1(\lambda^{-1}) & Y_2^1(\lambda^{-1}) & Y_3^1(\lambda^{-1}) & Y_4^1(\lambda^{-1}) \\ Y_1^2(\lambda^{-1}) & Y_2^2(\lambda^{-1}) & Y_3^2(\lambda^{-1}) & Y_4^2(\lambda^{-1}) \\ Y_1^1(1) & Y_2^1(1) & Y_3^1(1) & Y_4^1(1) \\ Y_1^2(1) & Y_2^2(1) & Y_3^2(1) & Y_4^2(1) \end{pmatrix}, \tag{10}$$

the boundary conditions lead to the equation $\det(\tilde{Y}) = 0$. Given β, λ, and ν we solve this equation to obtain the (dimensionless) energies $\epsilon_{j,i}(\nu)$ where j is the total angular momentum and i labels the different eigenstates for a fixed j, in such a way that for $\nu = 0$ and $\beta = 0$ we have $\epsilon_{j,i} < \epsilon_{j,i+1}$.

In order to fix numerical estimates for the parameters we consider characteristic values extracted from recent experiments performed on semiconductor heterostructures defined on a 2DEG. Rings with external radius $R \sim 400-500$ nm and an aspect ratio $\lambda \sim 2$ have been recently employed as devices.[14] Typical values for the Fermi wavelength are $\lambda_F \sim 40-50$ nm that give $k_F \sim 0.1$ nm^{-1}. For $R = 400$ nm one gets a maximum value of the (dimensionless) Fermi energy $\epsilon_F = (Rk_F)^2 \sim 1600$. For an effective mass $m \sim 0.042 m_e$, a Rashba coupling constant $\alpha = 8$ meV nm and $R \sim 400$ we obtain $\beta = 2000\ \text{nm}/R(\text{nm}) \sim 4$. These parameters define the sample **S** studied in the present work. As the relevant situation for an isolated system, we work in the canonical ensemble keeping fixed the total number of electrons N as the magnetic flux is varied. One can estimate N at zero flux,[23] that in this case gives $N = [3\ \epsilon_F/8] = 600$ (the symbol [..] denotes integer part). The maximum number of transverse channels M can be then calculated as[24]

$$M = \left[\frac{2\sqrt{N}(\lambda - 1)}{\pi\sqrt{\lambda^2 - 1}}\right]. \tag{11}$$

Thus for $N \sim 200-600$ one gets $M \sim 4-8$, in agreement with the reported experimental values.[13]

For $\nu = 0$ and finite β, the SO breaks the degeneracy between states differing in one unit of j. The degeneracy between states with opposite values of j is broken by the presence of a finite magnetic flux ν, the charge PC being the signature of this broken symmetry.

III. ENERGY LEVELS AND PERSISTENT CURRENTS

As discussed previously in the literature, in 1D rings the RSO induces a topological phase,[10] $\Delta_B = \alpha m/\hbar^2 \oint (\hat{z} \times \sigma) \cdot d\mathbf{l}$, that once added to the Bohm-Aharonov one $2\pi\nu$, leads to an "*effective flux*" $\nu_{\text{eff}} = \nu + \frac{1}{2}(1 \mp \sqrt{(2\alpha m a/\hbar^2) + 1})$ (the $\pm$ sign depends on the sign of the z spin projection in the *local spin frame* and a is the radius of the ring). It is then via this effective flux that the SO interaction affects the behavior of the PC.[11]

The situation in the 2D ring is considerably more involved. We display in Fig. 1 some regions of the spectrum for both $\beta = 0$ and $\beta = 4$ cases. The upper panel of Fig. 1 shows the lowest eigenvalues of the multichannel ring **S** as a function of ν. As the first transverse channel is active in that region, the spectrum is similar to that of the 1D ring (due to the symmetry with respect to $\nu = 0.5$, the spectrum is shown for $0 \leqslant \nu \leqslant 0.5$). We can observe the evolution with ν of the single particle energy states labeled by the quantum numbers (j, i). For $\beta = 0$ (bold dotted lines) we have the double degenerate fundamental states $(\pm 1/2, 0)$ and the doublets $(1/2, 1)$, $(3/2, 0)$ and $(-1/2, 1)$, $(-3/2, 0)$. Notice that at $\nu = 0$, except for the fundamental state, the others are four-fold degenerate and, as in the 1D regime, crossings occur only at $\nu = 0, 0.5$. The effect of a finite RSO coupling is clearly visible in the figure. The RSO interaction lowers the energy of each state and it can even change the order in which they appear. For the case shown in Fig. 1, the lowest energy states are $(3/2, 0)$ and $(-3/2, 0)$ that for finite flux remain almost degenerate and appear in the figure as a single line. We then have four states which for very small ν (i.e., before any ν induced level crossing) are ordered as $(-1/2, 0)$, $(1/2, 0)$, $(5/2, 0)$, $(-5/2, 0)$. Higher in energy, we display the states $(1/2, 1)$, $(-1/2, 1)$, $(-7/2, 0)$, $(7/2, 0)$. Notice that as a result of the RSO new crossings appear. As an example, we draw arrows in the panel as guides for the location of the new crossings between $(1/2, 0)$ and $(5/2, 0)$ and $(-1/2, 1)$, $(-7/2, 0)$. These crossings are indeed the fingerprints of the effective flux ν_{eff} mentioned above.[25]

When many transverse channels are activated, the spectrum displays additional crossings between levels belonging

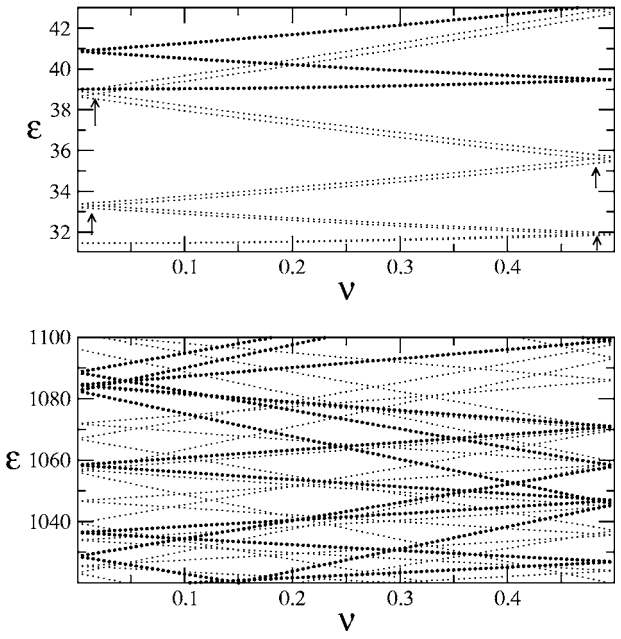

FIG. 1. Dimensionless energies ϵ as a function of the magnetic flux ν for the annular cavity **S** defined in the text. Upper panel: lowest eigenvalues in the absence of RSO (bold dotted lines) and for $\beta=4$ (small dotted lines). The arrows are guides for the eyes to locate the position of the crossings due to the RSO coupling. See the text for details. Lower panel: high energy region showing many crossings between different transverse channels, in the absence of RSO (bold dotted lines) and for $\beta=4$ (small dotted lines).

to different channels, even in the absence of RSO coupling (see lower panel of Fig. 1). The crossings that arise due to the SO interaction are mixed with the crossings between levels with different transverse channel numbers, and it is not straightforward to identify the signature of an effective flux as in the 1D case, when only a single transverse channel is active. This can be understood looking at the functional form of the 2D Hamiltonian Eq. (3), whose last term contains the ratio α/ρ between the RSO constant and the radial coordinate. Therefore, loosely speaking, on average each transverse channel feels a topological phase that depends on the value of the transverse quantum number. This argument could be extended to explain the difference in patterns of conductance oscillations of single-channel and multichannel open rings with RSO interaction.[16] In terms of the dimensionless variables, the only nonvanishing component of the charge current density for eigenstates as given in Eq. (4) reads

$$J_\varphi = \frac{e\hbar}{mR^3\xi}[(l-\nu)f_l^2 + (l+1-\nu)g_{l+1}^2 + \beta\xi f_l g_{l+1}]. \quad (12)$$

Employing the probability and spin densities, $\delta_j(\xi)\equiv f_l^2 + g_{l+1}^2$, $\langle\hat{\sigma}_z\rangle_j \equiv \Psi^\dagger\hat{\sigma}_z\Psi$ and $\langle\hat{\sigma}_\rho\rangle_j \equiv \Psi^\dagger\hat{\sigma}_\rho\Psi$, the current can be written as

$$J_\varphi = \frac{e\hbar}{mR^3\xi}\left((j-\nu)\delta_j(\xi) - \frac{1}{2}\langle\hat{\sigma}_z\rangle_j + \frac{\beta}{2}\langle\hat{\sigma}_\rho\rangle_j\xi\right). \quad (13)$$

Therefore the effect of the SO interaction in the charge current density is unveiled in the last term of Eq. (13). To calculate the total charge PC we have to sum the contributions of all states up to the Fermi energy

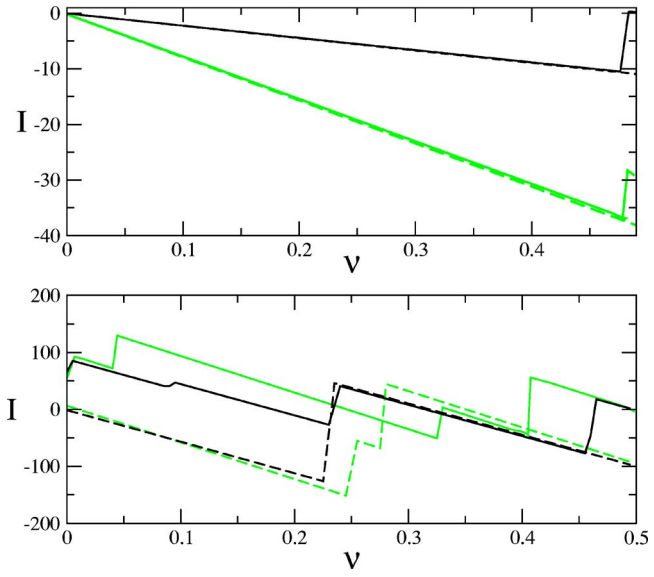

FIG. 2. (Color online) Persistent current I as a function of ν in the absence of SO interaction (dashed lines) and for $\beta=4$ (solid line). Upper panel corresponds to $N=6$ (black lines) and $N=22$ (grey lines) and $M=1$. The lower panel corresponds to $N=162$ (black lines) and $N=182$ (grey lines). The finite slope of the jumps is due to size of the flux step (5.10^{-3}) employed in the numerical calculations.

$$\tilde{I} = \int_r^R d\rho \sum J_\varphi^{(n)}(\rho) = -c\frac{\partial E}{\partial\phi}, \quad (14)$$

whereas before, n labels the occupied states. Besides a geometrical factor that takes into account the area of the outer circle of the sample $\tilde{I}$ is the magnetic moment. In terms of the dimensionless variables

$$\tilde{I} = \frac{cE_0}{\phi_0}I, \quad I = -\frac{\partial\epsilon}{\partial\nu}. \quad (15)$$

For the parameters quoted before for sample **S**, results $\tilde{I} \sim 0.2\, I(nA)$. In Fig. 2 we plot I as a function of ν for $\beta=4$ and for comparison, in the absence of RSO interaction. For $N=6$ and $N=22$, when only one channel is open ($M=1$), the jumps in the PC are solely due to SO interaction and are located, as for the 1D rings, at the same flux values independently of the filling (see the upper panel of Fig. 2). On the other hand, for $N=162(M=2)$ and $N=182(M=4)$ the location of the jumps in the PC depends strongly on the channel number, as it is shown in the lower panel of Fig. 2 and in accordance to our previous discussion.[26]

IV. SPIN ACCUMULATION EFFECT

As a result of the RSO interaction, spin projection is not a good quantum number. For N occupied states, the mean value of the z projection of the spin is proportional to

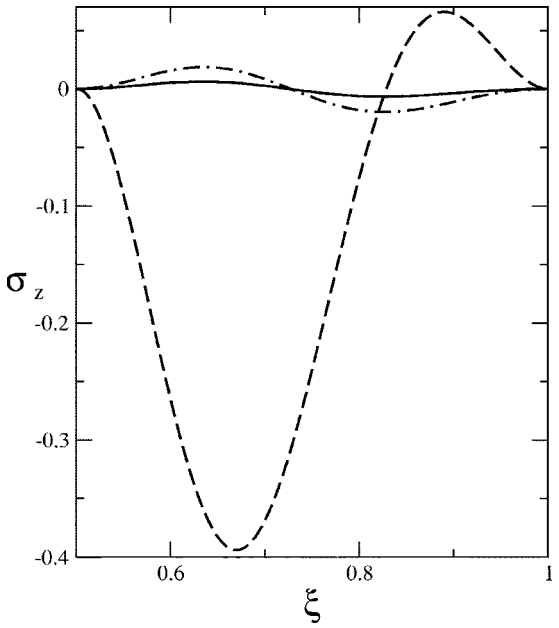

FIG. 3. Dimensionless total spin density σ_z as a function of ξ for $\nu=0.2$ for the sample **S**. $N=2$ (solid line), $N=4$ (dashed line), and $N=6$ (dotted-dashed line).

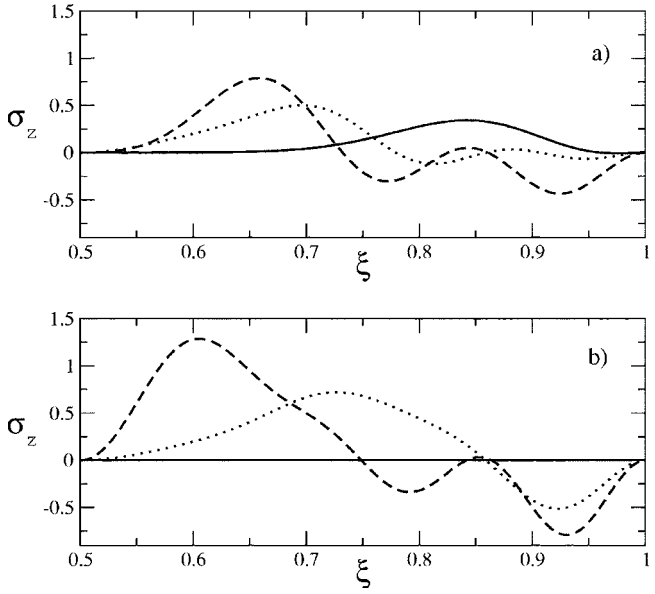

FIG. 4. Dimensionless total spin density σ_z as a function of ξ for $\nu=0$ (solid line), $\nu=0.1$ (dotted line), and $\nu=0.45$ (dashed line) for the sample **S**. (a) $N=181$, (b) $N=182$. Note that in this case $\sigma_z=0$ for $\nu=0$ as expected for an even number of particles.

$$\Sigma_z = \int_{\text{ring}} \sum_n \Psi_n^\dagger \hat{\sigma}_z \Psi_n = 2\pi \int_{1/\lambda}^{1} \sigma_z(\xi)\xi d\xi, \qquad (16)$$

where $n=1$, $N(\epsilon_F)$ labels the occupied states and $\sigma_z(\xi)$ corresponds to the total spin density for N particles. Even in the case of N even, a nonzero spin density is obtained when SO is present and $\nu \neq 0$. In addition a spin accumulation effect is developed and it is manifested in the tendency of σ_z to be positive on one border of the sample and negative on the other one. Although the accumulation becomes stronger as N and the number of open channels increase, it is also present when only one transverse channel is active. In order to explain the origin of the effect we first concentrate on a pair of eigenstates that, being degenerate at $\nu=0$ with opposite value of j and with opposite out-of-plane spin projection, become nondegenerated for finite ν. The expectation value of $\hat{\sigma}_z$ in a given Ψ_j is $\langle \hat{\sigma}_z \rangle_j = |f_{l-\nu}|^2 - |g_{l-\nu+1}|^2$. It is straightforward to verify that at $\nu=0$ states with opposite value of j have opposite value of $\langle \hat{\sigma}_z \rangle$ and therefore for even number of particles $N=2p$, is $\sigma_z(\xi)=0$. As $\nu>0$, two facts induce a spin accumulation effect. On one hand, the magnetic field breaks the symmetry between single particle states with opposite value of j and on the other hand, due to the presence of additional level crossings the total J_z of the ground state can change and be different from zero for finite flux. In Fig. 3, we show σ_z for $\beta=4$, $\nu=0.2$ and $N=2,4,6$. For $N=2$, the single particle states have $j=\pm 3/2$. As ν is turned on, the effective orbital index $l_{\text{eff}} \equiv l-\nu$ becomes $1-\nu$ and $-2-\nu$ for $j=3/2$ and $j=-3/2$, respectively. Thus as the modulus of the effective orbital index decreases (increases) for $j=3/2$ ($j=-3/2$), the probability density and $\langle \hat{\sigma}_z \rangle_{j(-j)}$ are pushed toward the internal (external) boundary of the sample. This symmetry breaking explains the observed accumulation effect in this case. For $N=4$ the situation is different. Due to the level crossing mentioned before, the single particle states in the ground state have $j=3/2,-3/2,-1/2,5/2$ and the accumulation effect is mainly due to the imbalance between the last two states. We show the case $N=6$, which again is similar to the case $N=2$.

As the particle number is increased to the relevant experimental values, transverse channels are activated and the description of the effect becomes more complicated. Nevertheless our simulations suggest that the accumulations effect is a generic feature of the system in the presence of a magnetic flux. As an illustration, in Fig. 4 we show the spin density σ_z as a function of the dimensionless coordinate ξ for $N=181$ and $N=182$ and different values of the magnetic flux in the range $0<\nu<0.5$. For $N=181$ and $\nu=0$ [see Fig. 4(a)] a finite $\sigma_z(\xi)$ is obtained whose value corresponds to the last occupied level, as expected for the odd particle number. On the other hand, for $N=182$ is $\sigma_z(\xi)=0$ at $\nu=0$, as it is shown in Fig. 4(b). For $\nu>0$ the spin density profile has a more complicated structure than in the quasi-1D regime due to the behavior of the radial components of the spinors as the number of transverse channels increases and the flux is varied.

V. CONCLUSIONS

In this paper we have shown that a finite magnetic flux threading a multichannel semiconductor ring with SO interaction induces spin polarization with opposite sign for the two borders of the ring. We believe this system constitutes a proposal to detect accumulation effects induced by SO interaction in constrain geometries in equilibrium, that is without applied electric fields or currents. The characteristic wavelength of the accumulation effect is of the order of 0.1 μm,

which is not far from the sensitivity of methods employed recently to probe spin polarization in semiconductor channels.[17] Besides the accumulation effect, the integrated spin density Σ_z is different from zero and is sensitive to the value of the magnetic flux, as can be inferred from Fig. 4. In the presence of an external magnetic field perturbation, the spin magnetization should be proportional to Σ_z. With the help of experimental techniques based on resonant methods it should be possible to sense changes in the total magnetization of isolated rings due to SO interaction.[27]

ACKNOWLEDGMENTS

Partial financial support by ANPCyT Grant No. 03-11609, CONICET, and Foundación Antorchas Grant No. 14248/113 are gratefully acknowledged. We would like to thank C. Balseiro and G. Usaj for helpful discussions. G.S.L thanks ICTP, Trieste, where part of this work was performed.

*Electronic address: lozano@df.uba.ar
†Electronic address: majo@cab.cnea.gov.ar

[1] *Semiconductor Spintronics and Quantum Computation*, edited by D. Awschalom, N. Samarth, and D. Loss (Springer, New York, 2002).
[2] A. F. Morpurgo, J. P. Heida, T. M. Klapwijk, and B. J. van Wees, Phys. Rev. Lett. **80**, 1050 (1998).
[3] J. Nitta, F. E. Meijer, and H. Takayanagi, Appl. Phys. Lett. **75**, 695 (1999).
[4] D. Frustaglia and K. Richter, Phys. Rev. B **69**, 235310 (2004).
[5] Y. Meir, Y. Gefen, and O. Entil-Wohlman, Phys. Rev. Lett. **63**, 798 (1989).
[6] D. Loss and P. M. Goldbart, Phys. Rev. B **45**, 13544 (1992).
[7] A. V. Balatsky and B. L. Althsuler, Phys. Rev. Lett. **70**, 1678 (1993).
[8] M. V. Berry, Proc. R. Soc. London, Ser. A **392**, 45 (1984).
[9] Y. A. Bychkov and E. I. Rashba, JETP Lett. **39**, 78 (1984).
[10] A. G. Aronov and Y. B. Lyanda-Geller, Phys. Rev. Lett. **70**, 343 (1993).
[11] A. V. Chaplik and L. I. MaGarill, Superlattices Microstruct. **18**, 321 (1995).
[12] J. Splettstoesser, M. Governale, and U. Zülicke, Phys. Rev. B **68**, 165341 (2003).
[13] D. Mailly, C. Chapelier, and A. Benoit, Phys. Rev. Lett. **70**, 2020 (1993).
[14] F. Meijer, A. Morpurgo, T. Klapwijk, T. Koga, and J. Nitta, Phys. Rev. B **69**, 035308 (2004).
[15] Jeng-Bang Yau, E. P. De Poortere, and M. Shayegan, Phys. Rev. Lett. **88**, 146801 (2002).
[16] S. Souma and B. K. Nikolíc, Phys. Rev. B **70**, 195346 (2004).
[17] Y. K. Kato, R. C. Myers, A. C. Gossard, and D. D. Awschalom, Science **306**, 1910 (2004).
[18] J. Sinova, D. Culcer, Q. Niu, N. A. Sinitsyn, T. Jungwirth, and A. H. MacDonald, Phys. Rev. Lett. **92**, 126603 (2004).
[19] J. Wunderlich, B. Kaestner, J. Sinova, and T. Jungwirth, Phys. Rev. Lett. **94**, 047204 (2005).
[20] G. Usaj and C. A. Balseiro, cond-mat/0405065 (unpublished).
[21] M. Abramowitz and I. A. Stegun, *Handbook of Mathematical Functions* (Dover, New York, 1972).
[22] E. Tsitsishvili, G. S. Lozano, and A. O. Gogolin, Phys. Rev. B **70**, 115316 (2004).
[23] M. Baltes and E. Hilf, *Spectra of Finite Systems* (Bibliographisches Institut, Mannheim, 1976).
[24] A. J. Fendrik and M. J. Sánchez, Eur. Phys. J. B **14**, 725 (2000).
[25] Assuming a ring of radius $\hat{R}=(R+r)/2$ and employing the dispersion relation $\epsilon(\nu_{\text{eff}})$ for 1D geometries (Ref. 10), it is straightforward to obtain the values of ν_c, given two levels with $j-1$ and $-j$ for example.
[26] In order to decrease CPU time in the numerical simulations, and without loss of generality, we employ for the present analysis these values of N. Although they are smaller that the ones that correspond to the experimental reported E_F, the results and conclusions are completely general, as many transverse channels ($M\sim 4$) are open.
[27] R. Deblock, R. Bel, B. Reulet, H. Bouchiat, and D. Mailly, Phys. Rev. Lett. **89**, 206803 (2002).